NASA Technical Paper 1081

Mechanical Behavior
and Fracture Characteristics
of Off-Axis Fiber Composites
I - Experimental Investigation

John H. Sinclair and Christos C. Chamis

DECEMBER 1977
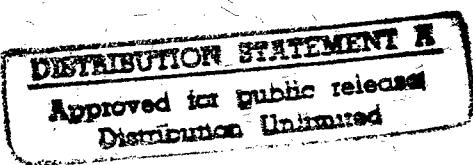
NASA

NASA Technical Paper 1081

Mechanical Behavior and Fracture Characteristics of Off-Axis Fiber Composites

I - Experimental Investigation

John H. Sinclair and Christos C. Chamis

Lewis Research Center
Cleveland, Ohio

NASA

National Aeronautics
and Space Administration

**Scientific and Technical
Information Office**

1977

MECHANICAL BEHAVIOR AND FRACTURE CHARACTERISTICS

OF OFF-AXIS FIBER COMPOSITES

I - EXPERIMENTAL INVESTIGATION

by John H. Sinclair and Christos C. Chamis

Lewis Research Center

SUMMARY

An experimental investigation was conducted to study the mechanical behavior and fracture characteristics of high-modulus graphite-fiber/epoxy, unidirectional composite subjected to off-axis tensile loads. The investigation included testing to failure unidirectional specimens whose material axes were oriented at various angles (0° to 90°) to the load direction, generating the stress-strain data to fracture from strain gages placed at various locations across the width of the specimen at midlength and near the end tab, and scanning electron microscopic examinations of specimen fracture surfaces.

The results show that the stress-strain curves to failure from all gage positions are linear. In-plane bending, caused by shear coupling, produces measured axial strain variations of about 6 percent from edge to edge of the specimen.

The fractured surfaces revealed three distinct fracture characteristics: irregular surface with fiber breaks and fiber pull-out near 0° load angle, regular surface with extensive matrix lacerations in the 5° to 30° load-angle range, and regular surface with extensive matrix cleavage in the 45° to 90° load-angle range. These observations led to the identification of single-stress predominant fracture modes and of distinct fracture surface characteristics associated with these modes and to the formulation of criteria for characterizing these fracture modes and their corresponding fracture surfaces.

The results of this investigation were used in the theoretical investigation and comparisons described in Part II (ref. 1). These results should also provide a firm basis for identifying, characterizing, and quantifying fracture modes in off-axis and angleplied laminates.

INTRODUCTION

Off-axis tensile data for unidirectional composites are of considerable interest to the fiber-composite community for several reasons. Some of these are (1) determination of the variation of elastic properties and fracture stress (strain) as a function of load angle (angle between fiber and load directions), (2) verification of composite macromechanics theories for elastic properties and for combined-stress fracture, and (3) generation of fundamental information for assessing angle-plied laminate mechanical behavior.

An investigation of the first two aspects dealing with boron-fiber/epoxy composites is reported in reference 2. A brief review of previous work is also covered in this reference. However, the third aspect has not been examined with respect to fracture modes, morphology of fracture surfaces, criteria for identifying these fracture modes, and convenient plotting procedures for quantifying them.

The objective of this investigation was to study the mechanical behavior and fracture characteristics of unidirectional, high-modulus, graphite-fiber composites subjected to off-axis tensile load. The focus of the investigation was on identifying fracture modes, on formulating criteria to characterize these modes and their associated fracture surfaces, and on developing convenient plotting techniques to quantify them.

The investigation included both experimental and theoretical parts. In the experimental part strain gages were used to measure the mechanical response of off-axis specimens tested in tension at various angles (0° to 90°) to the fiber direction. Also, the surface morphology of the fracture specimens were examined in detail by use of a scanning electron microscope (SEM). In the theoretical part composite mechanics was used to predict the elastic properties of the off-axis specimens. Finite elements, including NASTRAN, were used for the stress analysis and a combined-stress failure criterion was used to predict the fracture stress. The predicted results were subsequently compared with the measured data. Theoretical sensitivity studies were used to help explain anomalies in the experimental data. Sensitivity studies were also used to guide the development of convenient plots for quantifying fracture modes. Results for the experimental investigation are described herein. Those from the theoretical investigation and the comparisons are described in Part II.

A spinoff of this investigation was the evolution of the 10° off-axis tensile test for intralaminar shear characterization of unidirectional fiber composites (ref. 3).

LAMINATE FABRICATION

The composite, consisting of eight unidirectional plies of Modmor-I graphite fibers in a matrix of ERLA-4617 epoxy resin cured with meta-phenylene di-amine (MPDA), was

fabricated by a commercial vendor. This composite will be referred to as Mod I/E hereinafter. The vendor used the following curing procedure. The laminate was heated from room temperature to 121° C (250° F) under a partial vacuum of approximately 2 newtons per square centimeter (N/cm^2) (3 psi) and held for 40 minutes at this temperature. It was then heated to 177° C (350° F) under an autoclave pressure of 34.5 newtons per square centimeter (50 psi) and held for 2 hours. Pressure was maintained until it had cooled to 49° C (120° F).

SPECIMEN PREPARATION, INSTRUMENTATION, AND TESTING

A drafting machine was used to lay out tensile specimens at the desired load angles on the laminate plates (fig. 1). The specimens were then cut slightly over-width by a 0.061-centimeter (0.024-in.) thick diamond wheel mounted on a surface grinder. Stacks of specimens, so cut, were placed on edge and dressed down to the required 1.27-centimeter (0.500-in.) width by a diamond wheel. Specimen ends were reinforced with adhesively bonded fiber glass tabs. The final dimensions of the specimen were about 25.4 centimeter (10 in.) long, 1.27 centimeter (0.5 in.) wide, and about 0.142 centimeter (0.056 in.) thick.

Tensile specimens were instrumented with either 2 or 5 120-ohm, 60° delta-rosette strain gages arranged as shown in figure 2. The test specimens were placed in the grips pictured in figure 3 and loaded to fracture using a hydraulically actuated universal testing machine. Loading was incremental to facilitate periodic recording of strain gage data.

PREPARATION AND STUDY OF SCANNING ELECTRON MICROSCOPE SPECIMENS

Fractured surfaces of each tensile specimen were observed by scanning electron microscope, and typical photomicrographs were made to illustrate fracture modes.

Segments of tested laminates containing the fracture surfaces of interest were cut (while carefully preserving fracture surfaces) from each specimen and cemented (on edge with fracture surface up) to aluminum mounts. In order to facilitate observation by SEM, the specimens were made electrically conductive by coating them with a gold-palladium film, approximately 200 Å (20 nm) thick, which was applied by vapor deposition in a vacuum evaporator. They were then studied and photographed with a JUL-JSM-2 scanning electron microscope.

It is noted that only one specimen was tested at each orientation. The main reason for this was to minimize fabrication-variable effects on the measured data. The number of specimens that could be made from a single laminate was determined by laminate

size, which in this case was limited to a square, 30.5 centimeters (12.0 in.) on a side (fig. 1). Past experience has shown that the effects of orientation are more readily identified by testing specimens from the same laminate at several orientations rather than testing replicates (from the same laminate) at a given orientation and then selecting specimens from different laminates for the different orientations.

EXPERIMENTAL RESULTS AND DISCUSSION

The experimental results consist of stress-strain data, axial strain variations across tensile specimens at midlength and tab ends, fracture stresses and strains, combined plots, SEM photographs of fracture surfaces and macrophotographs of fractured specimens.

Stress-Strain Data

The strain-gage data reduction program (SGDR) (ref. 4) was used to generate stress-strain curves from the incremental loads and corresponding data recorded from strain gages. Three types of curves were generated: structural axes stresses σ_{cxx}, Poisson's strains ϵ_{cyy}, and the coupled shear strains ϵ_{cxy} as functions of axial strains ϵ_{cxx}. These curves are presented in figures 4 to 12. Specimens tested at 10°, 30°, and 60° from the fiber direction each had five gages, and all others (0°, 5°, 15°, 45°, 75°, and 90° off-axis specimens) had two gages. The two gage arrangements are pictured in figure 2. The figures (4 to 12) show curves for all of the gage positions for any given specimen superimposed on one plot.

The collective observations from the curves in figures 4 to 12 are these: The curves are essentially linear; there is relatively small scatter in the slopes of the stress-strain curves from the various gage sites; and the coupled shear strains are negligible at load angles near 0° and 90°. There is some deviation in the slopes of the Poisson's strain curves between center and end-tab gages at the specimen edges. This indicates the effect of end restraint on the Poisson's strain.

Strains were measured at midlength and near an end tab for all specimens. The axial strains at fracture (ε_{cxx}) range from approximately 0.19 to 0.50 percent. There appears to be no orderly pattern with regard to whether greater elongation occurred near the tab or at midlength. The center gage, located at specimen midlength, is used as a reference to which the other gages on a given specimen are compared. This gage is believed to be least susceptible to eccentricities, coupling shear effect, and Poisson's effect. It is, therefore, believed to give results most representative of the average state. Using this center gage as a standard, the axial strains measured at other sites

4

on the specimens lie between 0.8 and 1.4 times that of the center gage.

Specimen with five gages. - Specimens tested at 10°, 30°, and 60° off-axis each had five strain gages arranged as shown in figure 2 in order to measure strain variations across the width of the specimens. The stress-strain curves for these specimens are presented in figures 6, 8, and 10. The fracture strains $\mathscr{E}_{cxx}$ at the gage sites of these specimens range from 99 percent to 117 percent of the strains measured by the center gages.

As can be seen in figure 6(a), the magnitude of the strains at a given axial stress for the 10° off-axis specimen do not vary greatly from site to site. For example, at a stress of 2.1×10^4 newtons per square centimeter (30 ksi), the strain at the midlength center of the specimen (gage 2) is about 0.17 percent, and the strains near the edges midlength (gages 1 and 3) are around 0.19 percent. Since the edges of the specimen at midlength appear to have elongated a little more than the center, it is possible that the specimen twisted somewhat out of plane during the tensile test.

The 30° off-axis specimen showed fairly uniform elongation across the specimen width at midlength (0.29 to 0.30 percent at a stress of 6.9×10^3 N/cm^2 (10 ksi)), but the strain is higher near the tab end (0.32 to 0.34 percent at the same stress). (See figure 8(a).)

The fracture strains measured at the five gage sites for the 60° off-axis specimen ranged from approximately 0.41 percent to 0.44 percent (fig. 10(a)).

Figure 6(b) shows Poisson's strains as a function of axial strains for the 10° off-axis specimen. They range between 0.45 and 0.085 percent. At any level of axial strain ϵ_{cxx}, it can be seen that the Poisson's strains ϵ_{cyy} are larger at the specimen edges than at the center. Note that the difference is magnified because of the large scale on the ordinate. This is true both near the tabs and at the specimen midlength. The cause for this behavior is probably due to coupling between normal, shear strains, and transverse strain in the presence of the possible out-of-plane twisting mentioned previously. The Poisson's strains at fracture for the gage sites on the 30° off-axis specimen lie between approximately 0.062 and 0.089 percent (fig. 8(b)) and those for the 60° off-axis specimen range from about 0.03 to 0.04 percent (fig. 10(b)).

The coupled shear-strains are shown in figures 6(c), 8(c), and 10(c) as a function of the axial strains for the 10°, 30°, and 60° off-axis specimens, respectively. They do not appear to vary much from gage site to gage site and may be within the limits of experimental error.

Specimens with two gages. - The longitudinal specimen (0° off-axis), transverse specimen (90° off-axis), and specimens tested at 5°, 15°, 45°, and 75° with respect to the fiber direction each had two strain gages arranged on the specimens as shown in figure 2(a). The stress-strain curves for these specimens are presented in figures 4, 5, 7, 9, 11, and 12. The tensile fracture strains near the grips of these specimens range from 80 percent to 140 percent of the fracture strains at the specimen midlengths.

The fracture stress ($S_{\ell 11T}$) of the longitudinal tensile specimen (0° off-axis) was 56.3 newtons per square centimeter (81.7 ksi), and the gage near the tensile grip recorded a strain of 0.22 percent or 96 percent of the midlength gage, which gave a strain measurement of 0.23 percent.

Axial strains at fracture measured at the tab end and at the midlength of the 5° off-axis specimen (fig. 5(a)) did not agree as closely as they had in the 0° case. The specimen fractured at a stress of 38.1×10^3 newtons per square centimeter (55.2 ksi). The gage near the specimen grip indicated a strain of 0.250 percent, which is 1.35 times the 0.185 percent strain shown by the midlength gage. It was observed that the specimen thickness beneath the gage near the tab end was 0.138 centimeter (0.0542 in.), the thinnest area measured on the specimen, whereas that beneath the midlength gage was 0.141 centimeter (0.0556 in.).

The thickness variation probably contributes a small part to this relatively large difference. The major contribution is suspected to be from out-of-plane eccentricities. The contributions from both thickness variations and out-of-plane eccentricities were investigated using finite-element analysis. The details are described in the finite-element analysis section of Part II.

Tab-end strains for the specimens tested at 15°, 45°, and 75° off-axis had magnitudes between 0.24 and 0.45 percent and did not vary from midlength strains by more than 18 percent (figs. 7(a), 9(a), and 11(a)), but the transverse specimen (90° off-axis) had a tab end strain of 0.50 percent, which is 139 percent of the midlength strain of 0.36 percent (see fig. 12(a)). The cause for this difference is probably nonuniformities in the laminate due to out-of-plane eccentricities.

The Poisson's strains for the two-gaged specimens (0°, 5°, 15°, 45°, 75°, and 90° off-axis specimens) lie between 0.005 and 0.09 percent, and there is no regular pattern as to whether the larger strains occurred at tab-end or midlength (parts (b) of figs. 4, 5, 7, 9, 11, and 12).

The coupled shear strains for this group of specimens lie between 0.08 percent and 0.74 percent. Again, the larger values for a given specimen are found sometimes at the tab end and sometimes at the midlength (parts (c) of figs. 5, 7, 9, and 11).

The unidirectional composite properties (longitudinal, transverse, and intralaminar shear) measured in this investigation are compared with those supplied by the material manufacturer in table I. The data from the center gage only is used in these comparisons.

The measured data from the center gage for all the specimens is summarized in table II. The data shown in this table include modulus along the load direction, Poisson's ratio, coupling coefficient (between shear and extension), fracture stress, and fracture strain.

6

Strain Variation Across Specimens at Midlengths and Tab Ends

Axial strains at fracture are shown in figure 13 for specimens tested at load angles of 10°, 30°, and 60° from the fiber direction (five gage specimens). These data points, taken directly from the measured stress-strain data, are accompanied by a schematic of the specimens and plots of strain against gage location.

For the 10° off-axis specimen the experimentally measured fracture strains are higher at the specimen edges than at the center (0.320 percent and 0.336 percent compared with 0.287 percent) for the gages located at the midlength. Near the tensile grips, however, the strain was higher halfway across the specimen (0.305 percent) than near the edge (0.288 percent). It is suspected that these differences are due primarily to the restraining effects of the grips. The important point to observe is that the difference between the axial strains at the edges (at the specimen midlength) is less than 5 percent. At the tab end the strains are very close to those measured at midlength. The 0.288 percent at the specimen edge and 0.305 percent halfway across the specimen lie within the strain range measured at the midlength of the specimen.

For the 30° off-axis specimen the fracture strain at midlength measured 0.365 percent at one specimen edge, 0.365 at the center, and 0.380 at the other edge. Near the grips, however, the strains were 0.395 percent at the specimen edge and 0.424 percent halfway across the specimen (fig. 13). As mentioned previously, the difference is suspected to be due to possible out-of-plane eccentricities.

The 60° off-axis specimen shows a narrow range of strains measured at the five gage sites. At the specimen midlength edges, the experimentally measured fracture strains are 0.417 and 0.440 percent, while halfway across the specimen the fracture strain is 0.414 percent. Near the grip the fracture strain was 0.406 percent at the specimen edge and 0.421 percent halfway across the specimen. As with the 10° off-axis specimen, the fracture strains at midlength are higher at the specimen edges than the halfway across the specimen, while near the grips the strain halfway across the specimen exceeds that near the specimen edge. Strain variation among the five gages on the 60° off-axis specimen is less than that observed for the 10° off-axis specimen (see fig. 13).

The fractured specimens are shown in figure 14. The fracture of a five-gage instrumented specimen is shown in figure 15. Note in figure 14 that the specimens tested at 0°, 5°, 10°, 15°, and 30° off-axis fractured away from the end tabs and those tested at 45°, 60°, 75° and 90° fractured near the end tab. Fractures occurring at or near end tabs are to be expected. Finite-element analyses results to be discussed in Part II show that the stresses at the edge near the end tab are higher than at the center in certain orientations. Consequently, these stresses can initiate fractures near the end-tab region. This leads to the interpretations that the fracture stresses of specimens that fractured near the end tabs are on the conservative side. Therefore, the axial stress

calculated from P/A (fracture load/cross-section area) is a reasonable representation of the axial stress.

Scanning Electron Microscope Study Results

The fractured surfaces of the specimens were examined using a scanning electron microscope to identify regions of distinct or predominant fracture modes associated with the different load angles. SEM photomicrographs of all the specimens tested are presented in figures 16 to 24. Each figure shows photomicrographs of three progressively larger magnifications (parts (a), (b), and (c)).

The fracture surface of the 0° specimen is shown in figure 16(a), where it can be observed that the fracture surface is irregular. An area replete with pulled-out fibers that broke off at varying lengths can be observed in the left foreground of the figure. This type of fracture suggests poor bonding between matrix and fibers. The remaining areas of figure 16(a) show irregularly shaped tiered or stepped surfaces that are typical of most of the fracture surface of specimens tested in longitudinal tension. At some regions fibers over relatively large areas fractured at approximately the same level, and they show little fiber pull-out. This type of surface is enlarged in figures 16(b) and (c). There was strong bonding between the fibers and matrix in these areas. The fracture mode of the resin was cleavage (fig. 16(c)). Lateral fiber surfaces of these stepped zones show some evidence of sheared resin lying between the fibers as seen in the upper left of figure 16(c).

The fracture surface in figure 16(c) reveals several distinct features. These features and some significant implications following therefrom are as follows:

(1) The fiber fracture surface is irregular but appears to be symmetric from the perimeter towards the center. This type of fiber fracture surface morphology will be considered to be typical of tensile fracture.

(2) The matrix fracture surface between fibers at the same level is smooth, indicating tensile brittle fracture by cleavage.

(3) The matrix fracture surface between fibers at different levels is lacerated, indicating fracture by tear, which will be considered to be fracture by intralaminar shear.

(4) The surface of fibers that pulled out appears to be clear of matrix residue, in general. This indicates weak interfacial bonding which may be construed to imply that the interfacial bond is predominantly mechanical.

(5) The transverse split in the left foreground is probably caused by the elastic energy release after fracture backlash.

The fracture surface of the 5° off-axis tensile specimen (fig. 17) reveals the following features:

(1) Surface tiering (fig. 17(b)) and matrix cleavage (fig. 17(c) both of which are indicative of tensile fracture

(2) Extensive matrix surface lacerations, indicating substantial fracture by intralaminar shear

(3) Fiber pull-out and fiber surfaces free of matrix residue, indicating weak interfacial bonding.

Recall that all of these features were observed in the fracture surface of the 0° tensile specimen.

The fracture of the 10° off-axis tensile specimen (fig. 18) reveals (1) matrix surface lacerations and (2) fiber surfaces free of matrix residue. Both of these features indicate that a different fracture mode became active. We will consider this mode to be induced by intralaminar shear stress. It is this observation and the theoretical considerations to be described in Part II that led to the recommendation that the 10° off-axis tensile specimen is suitable for intralaminar shear characterization of unidirectional fiber composites.

The fracture surfaces of the 15° and 30° off-axis tensile specimens (figs. 19 and 20) reveal similar features to those of the 10° off-axis tensile specimen. These surfaces, too, indicate that fracture was induced mainly by intralaminar shear stress.

The fracture surface of the 45° off-axis specimen (fig. 21) reveals the following features:

(1) Matrix cleavage with irregular boundary, indicating some transverse tensile fracture

(2) Matrix debris resulting probably from tensile matrix fracture

(3) Some matrix lacerations, indicating some intralaminar shear stress fracture.

These surface fracture features show that another fracture mode becomes active somewhere between a load angle of 30° and 45°. This mode is construed to have been induced by the transverse tensile stress.

The fracture surfaces of the 60° off-axis tensile specimen (fig. 22) and the 75° specimen (fig. 23) reveal mainly matrix cleavage and some fiber surface free of matrix residue; both of these features indicate that fracture was induced by transverse tensile stress.

The fracture surface of the 90° tensile specimen (fig. 24) reveals the following features:

(1) Matrix cleavage, indicative of tensile fracture of brittle materials

(2) Fiber surfaces free of matrix residue, indicative of weak interfacial bond, as was already mentioned

(3) Some matrix lacerations, indicating shear fracture at surfaces connecting two different levels.

These features indicate that transverse tensile stress produces fracture surfaces characterized by (1) matrix cleavage and (2) fiber surfaces clear of matrix residue.

The discussion dealing with the photomicrographs leads to the following criteria for studying and classifying fracture and fracture surfaces in Mod I/E composites.

(1) Fiber tensile fracture - The surface form is tiered and is characterized by the following:

      (a) Irregular fiber surface with some symmetry from the perimeter inward

      (b) Matrix cleavage surface

      (c) Fiber pull-out with fiber surfaces clear of matrix residue

      (d) Some matrix lacerations on interfiber surfaces connecting two different tier levels

      (e) Fiber fracture appears to occur at load angles near 0° and possibly up to 5°

(2) Intralaminar shear stress fracture - the fracture surface produced by this stress is mainly level or plane and is characterized by the following:

      (a) Extensive matrix lacerations

      (b) Fiber surfaces free of matrix residue

      (c) Intralaminar shear stress that appear to induce fracture, or contribute to it, at the load angle range $5^{\circ} < \theta \le 45^{\circ}$.

(3) Transverse tensile stress fracture - The fracture surface produced by this stress is level and is characterized by the following:

      (a) Matrix cleavage

      (b) Fiber surfaces free of matrix residue

      (c) Some matrix debris

      (d) Transverse tensile stress that appears to contribute to and induce fracture in the load angle range $45 \le \theta \le 90^{\circ}$.

(4) Mixed mode fracture - The fracture surface produced by mixed mode fracture is regular and is characterized by a mixture of lacerated and cleavaged matrix surfaces as well as fiber surfaces free of matrix residue.

These surface characteristics are produced by combinations of intralaminar shear and transverse tensile fracture as was already discussed. Mixed mode fracture based on these SEM results is probably prevalent in the load angle range somewhere between 15° and 30° to 45°. More definite limits are established in the theoretical section discussed in Part II.

The four criteria stated and the physical characteristics associated with them have not been reported previously. These should provide researchers with a set of definite guidelines for identifying and classifying fracture in graphite-fiber/resin-matrix composites. And, since the matrix appears to dominate fracture in the range $5^{\circ} < \theta \le 90^{\circ}$ via either intralaminar shear or transverse tensile, the preceding criteria should be applicable to all fiber/resin-matrix composites with longitudinal-to-transverse and longitudinal-to-intralaminar shear strength ratios of 2 or greater. For strength ratios

less than 2, the matrix tensile strength appears to govern fracture based on theoretical predictions.

The results obtained and discussed herein are used in the theoretical investigation and comparisons described in Part II (ref. 1).

SUMMARY OF RESULTS AND CONCLUSIONS

The major results of an experimental investigation to study the mechanical behavior and fracture characteristics of Mod I/epoxy fiber composites subjected to off-axis tensile loadings are

1. The stress-strain curves to fracture are linear. Strain gages located at different places on the specimen yielded approximately the same results. There is an axial strain variation across the specimen width due to in-plane bending.

2. Fracture surfaces of off-axis tensile specimens, examined by scanning electron microscope, exhibit distinct morphological characteristics:

    a. Irregular with fiber pull-out near load angle of 0° to the fiber direction

    b. Extensive amount of matrix lacerations in the load angle range $5^O < \theta < 30^O$.

    c. Matrix cleavage in the load angle range $45^O \le \theta \le 90^O$

    d. Combinations of matrix lacerations and cleavages in the load angle range $30^O < \theta < 45^O$

3. Criteria were established for characterizing fracture surfaces and identifying the corresponding predominant fracture mode in off-axis tensile specimens:

    a. Longitudinal tensile stress fracture - irregular fracture surface with fiber pull-out

    b. Intralaminar shear stress fracture - regular fracture surface with extensive matrix lacerations

    c. Transverse tensile stress fracture - regular fracture surface with extensive matrix cleavage.

4. The predominant fracture modes and associated load angle ranges of off-axis tensile specimens were identified:

    a. Longitudinal tensile (fiber breaks) near 0° load angle

    b. Intralaminar shear (matrix shear fracture) in the 5° to 30° load angle range

    c. Transverse tensile (matrix tensile fracture) in the 45° to 90° load angle range

    d. Mixed mode (transverse tensile and intralaminar shear) in the 30° to 45° load angle range.

5. The results of this investigation together with those in Part II should provide a good foundation for identifying, characterizing, and quantifying fracture modes in off-axis and angle-plied laminates.

Lewis Research Center,
    National Aeronautics and Space Administration,
        Cleveland, Ohio, August 22, 1977,
            506-17.

<div align="center">REFERENCES</div>

1. Chamis, Christos C.; and Sinclair, John H.: Mechanical Behavior and Fracture Characteristics of Off-Axis Fiber Composites. II - Theory and Comparisons. NASA TP-1082, 1977.

2. Sandhu, R. S.: Nonlinear Behavior of Unidirectional and Angle Ply Laminates. J. Aircr., vol. 13, no. 2, Feb. 1976, pp. 104-111.

3. Chamis, Christos C.; and Sinclair, John H.: 10° Off-Axis Tensile Test for Intralaminar Shear Characterization of Fiber Composites. NASA TN D-8215, 1976.

4. Chamis, C. C.; Kring, J.; and Sullivan, T. L.: Automated Testing Data Reduction Computer Program. NASA TM X-68050, 1972.

TABLE I. - UNIDIRECTIONAL COMPOSITE PROPERTIES

Property	Manufacturer's date	Lewis Research Center data[a]
Longitudinal tensile:		
Strength, $S_{\ell 11T}$, N/cm^2 (ksi)	53.75×10^3 (78.0)	56.3×10^3 (81.7)
Modulus, $E_{\ell 11T}$, N/cm^2 (psi)	22.5×10^6 (32.6×10^6)	24.1×10^6 (34.9×10^6)
Poisson's ratio, $\nu_{\ell 12}$	0.184	0.27
Transverse tensile:		
Strength, $S_{\ell 22T}$, N/cm^2 (ksi)	4.07×10^3 (5.82)	2.8×10^3 (4.0)
Modulus, $E_{\ell 22T}$, N/cm^2 (psi)	0.76×10^6 (1.10×10^6)	0.772×10^6 (1.12×10^6)
Poisson's ratio, $\nu_{\ell 21}$	0.0039	0.01
Longitudinal compression:		
Strength, $S_{\ell 11C}$, N/cm^2 (ksi)	45.6×10^3 (66.2)	--------------------
Modulus, $E_{\ell 11C}$, N/cm^2 (psi)	35.8×10^6 (52×10^6)	--------------------
Poisson's ratio	0.31	--------------------
Transverse compression:		
Strength, $S_{\ell 22C}$, N/cm^2 (ksi)	20×10^3 (29)	--------------------
Modulus, $E_{\ell 22C}$, N/cm^2 (psi)	1.25×10^6 (1.82×10^6)	--------------------
Poisson'ratio	0.0083	--------------------
Shear:		
Strength, $S_{\ell 12S}$, N/cm^2 (ksi)	4.49×10^3 (6.52)	5.51×10^3 (8.0)
Modulus, $G_{\ell 12}$, N/cm^2 (psi)	0.489×10^6 (0.709×10^6)	0.610×10^6 (0.89×10^6)

[a]Center gage.

TABLE II. - SUMMARY OF MEASURED DATA MODMOR I/EPOXY CENTER GAGE

Specimen	Load angle, deg	Specimen[a] thickness		Fracture load		Fracture stress		Fracture strain, $\mathscr{E}_{xx}$, percent	Modulus[b]		Poisson's[b] ratio	Coupling[b] coefficient
		cm	in.	N	lb	N/cm^2	ksi		N/cm^2	psi		
A-0	0	0.135	0.053	9572	2152	56.3×10^3	81.7	0.231	24.1×10^6	34.9×10^6	0.27	0
A-5	5	.142	.056	6850	1540	38.0	55.2	.188	20.2	29.3	.22	2.8
A-10	10	.142	.056	6183	1390	34.3	49.8	.286	12.3	17.8	.16	3.3
A-15	15	.142	.056	3550	798	19.8	28.7	.284	7.18	10.4	.20	2.6
A-30	30	.145	.057	1588	357	8.8	12.7	.365	2.41	3.49	.19	1.4
A-45	45	.142	.056	934	210	5.0	7.5	.390	1.36	1.97	.19	.82
A-60	60	.142	.056	712	160	3.9	5.7	.413	.305	1.31	.09	.38
A-75	75	.145	.057	569	128	3.1	4.5	.385	.829	1.20	.05	.21
A-90	90	.132	.052	463	104	2.8	4.0	.364	.772	1.12	.01	0

[a]Nominal specimen width, 1.27 cm (0.500 in.).
[b]These are slopes of straight lines fitted through the experimental data using least squares.
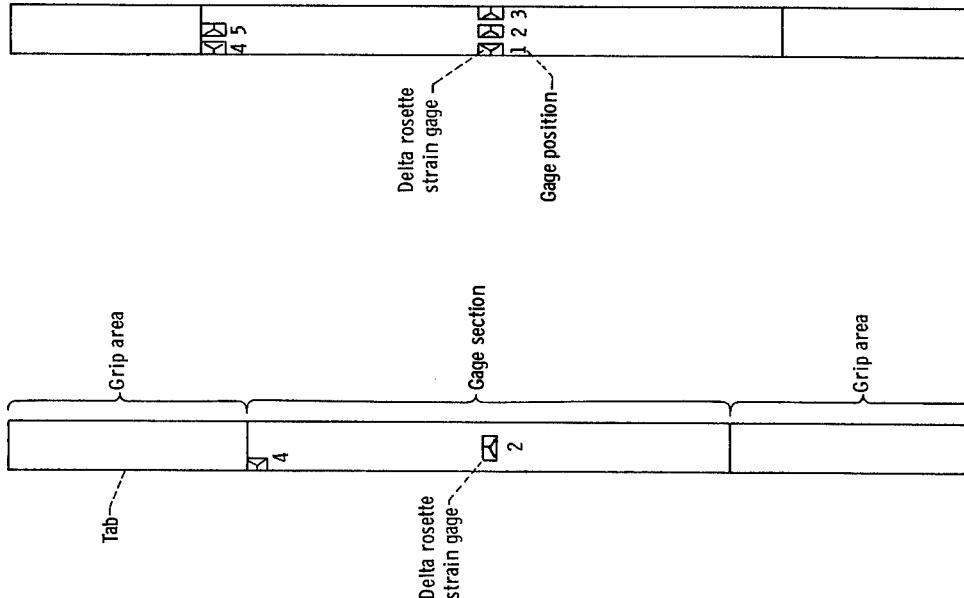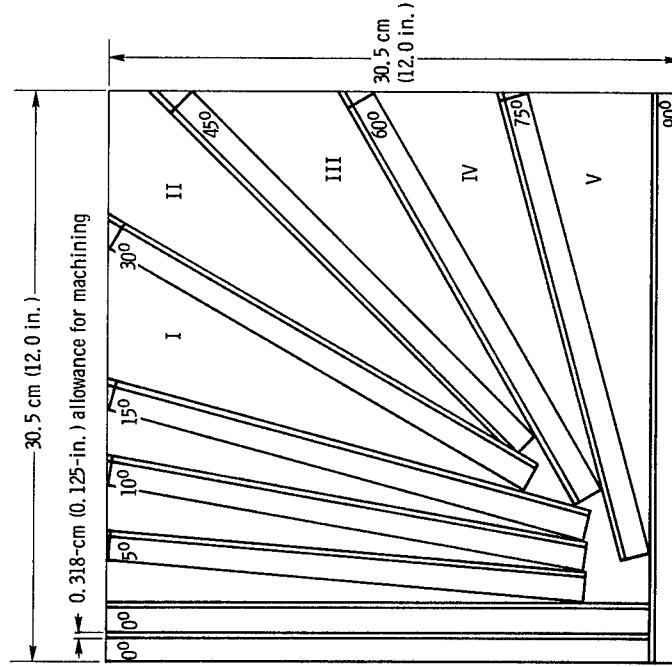
(a) Two-gage specimen.

(b) Five-gage specimen.

Figure 2. – Schematic of specimen geometry and strain-gage arrangement.

Figure 1. – Specimen layout on Mod I/E composite laminate plate.

Specimen
alinement
groove

Shim
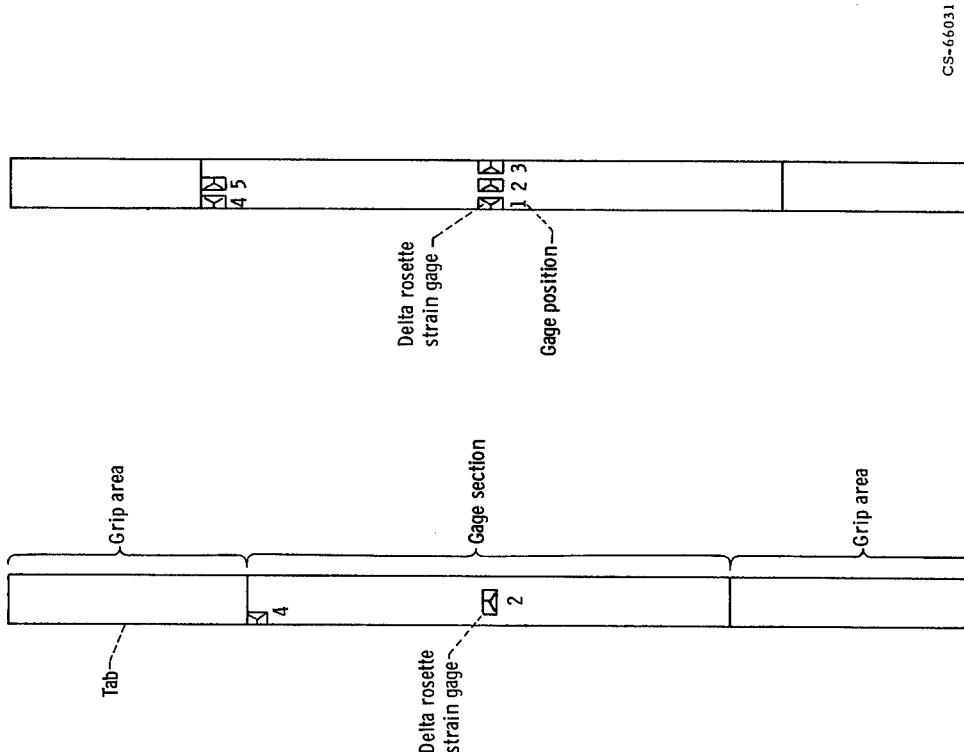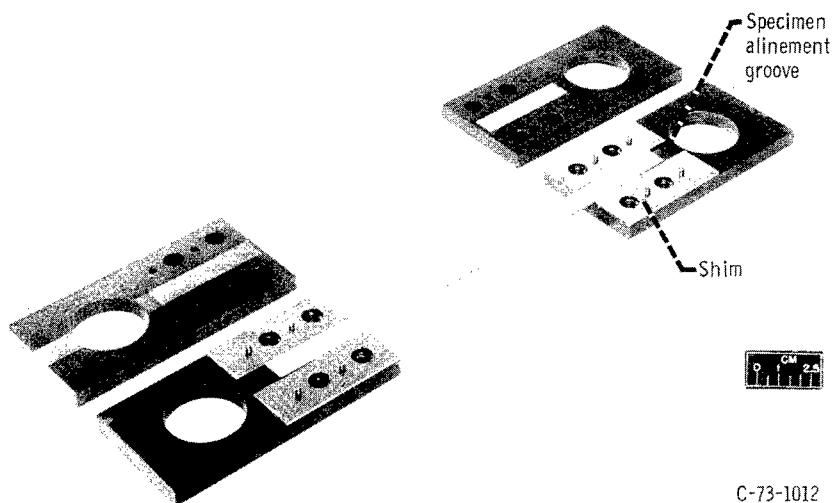
C-73-1012

(a) Grips disassembled.
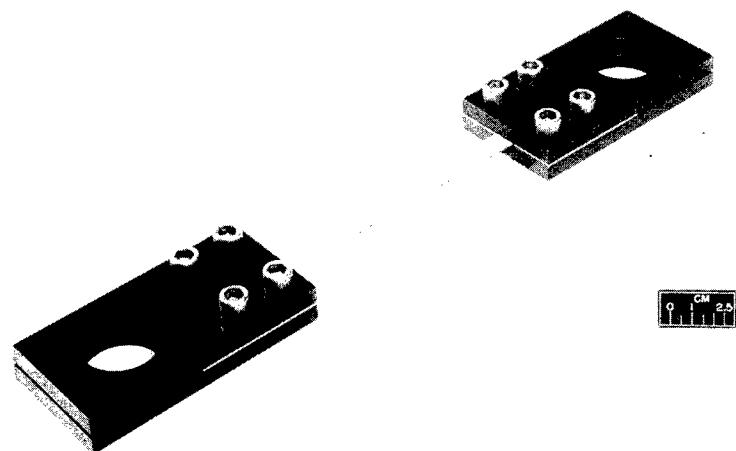
C-73-1011

(b) Grips assembled.

Figure 3. – Grips for composite tensile specimens.

(a) Stress-strain curves.

(b) Transverse (Poisson) strain curves.

(c) Shear strain curves.
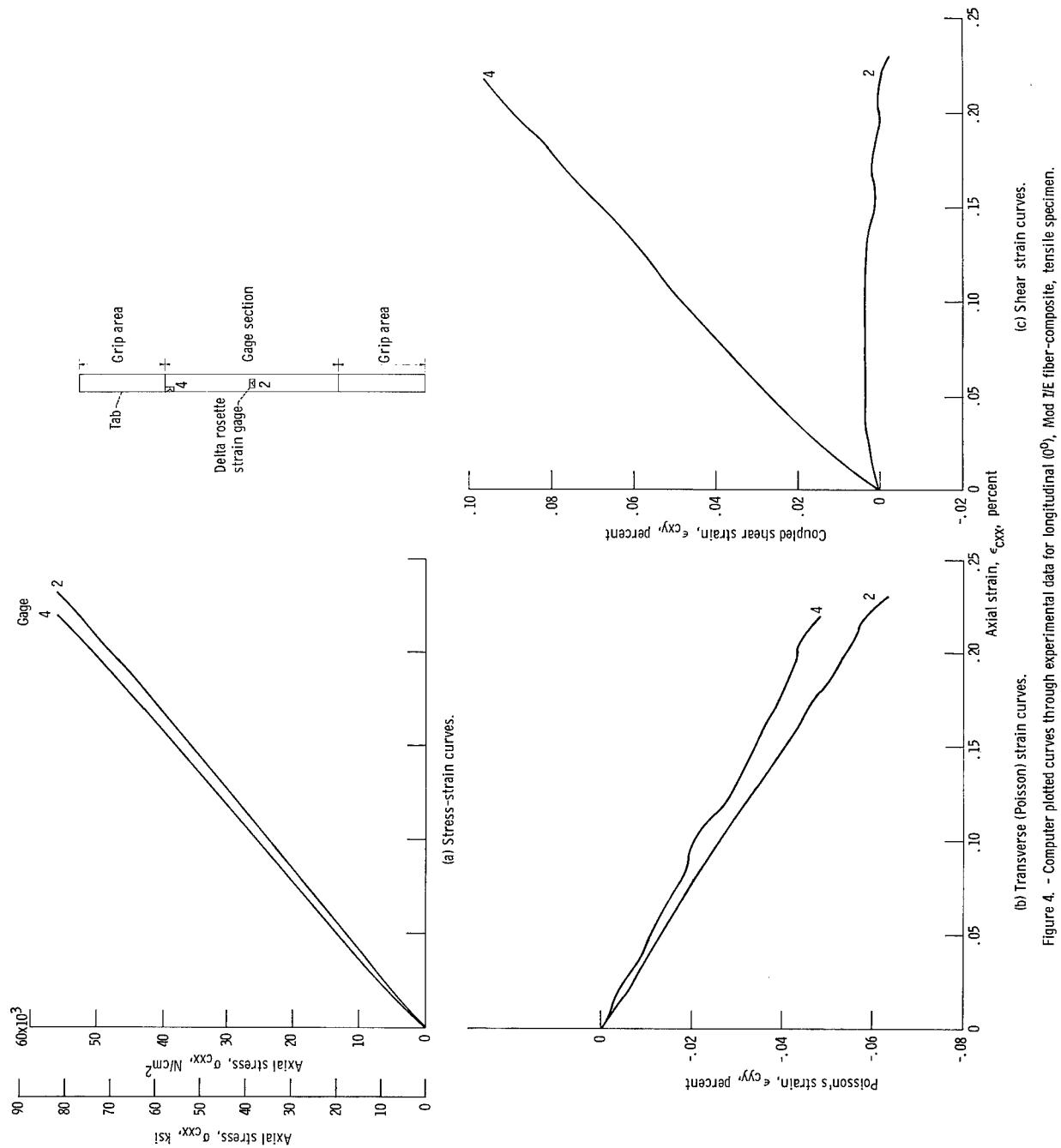
Figure 4. - Computer plotted curves through experimental data for longitudinal (0^0), Mod 7/E fiber-composite, tensile specimen.

(a) Stress-strain curves.

(b) Transverse (Poisson) strain curves.

(c) Shear strain curves.
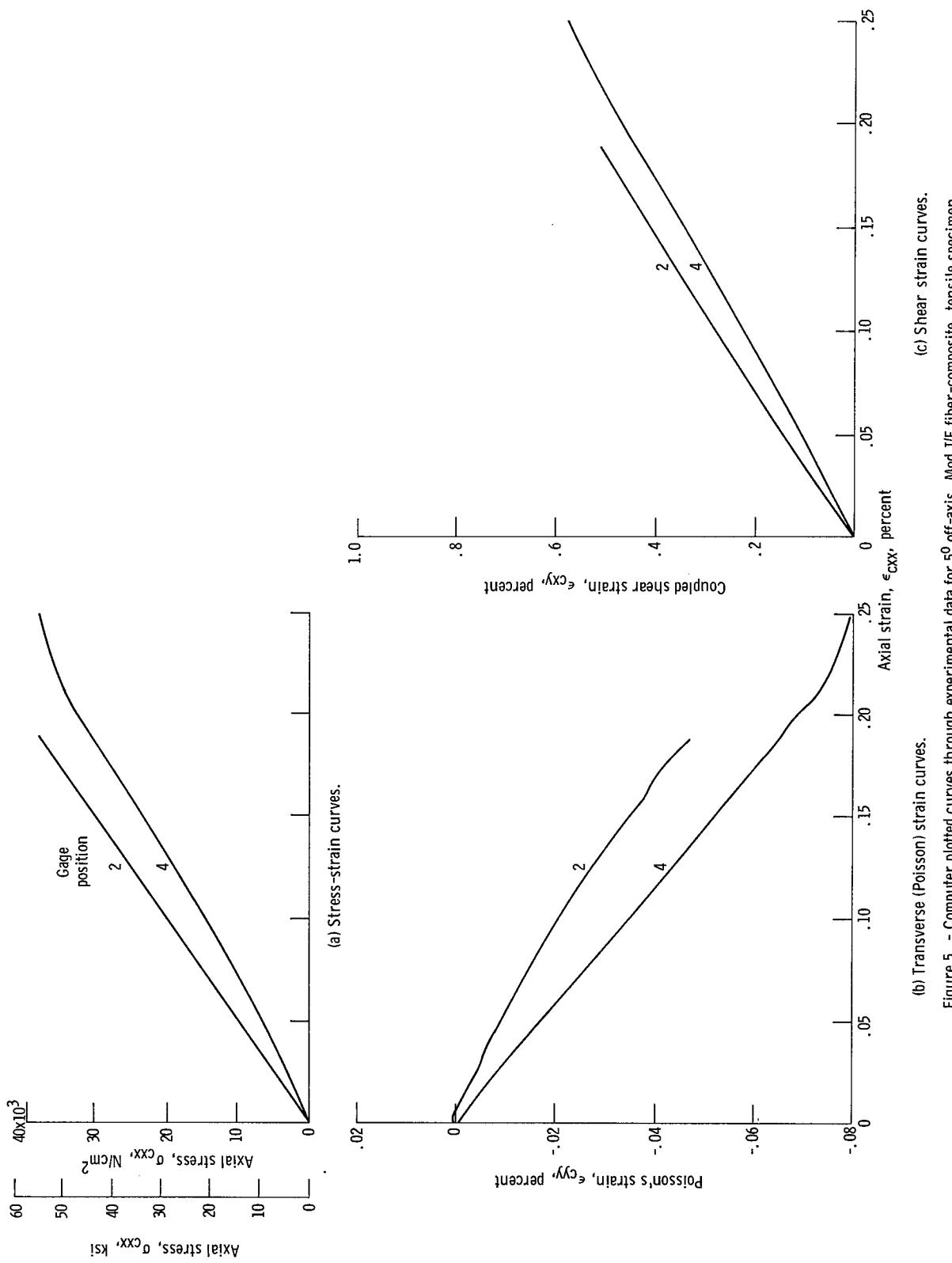
Figure 5. – Computer plotted curves through experimental data for 5^0 off-axis, Mod I/E fiber-composite, tensile specimen.

17

(a) Stress-strain curves.

(b) Transverse (Poisson) strain curves.

(c) Shear strain curves.
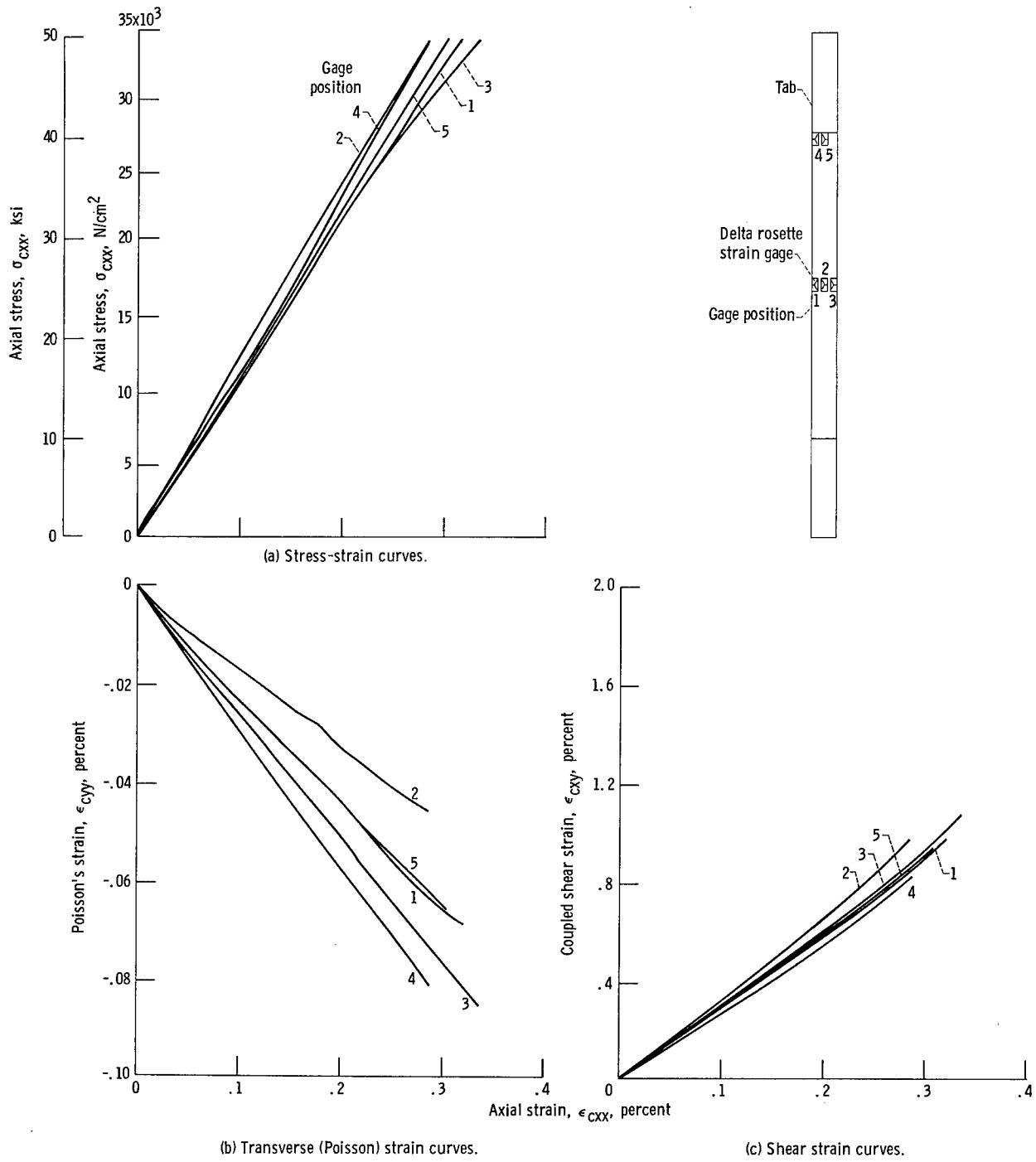
Figure 6. – Computer plotted curves through experimental data for 10^0 off-axis, Mod I/E fiber-composite, tensile specimen.
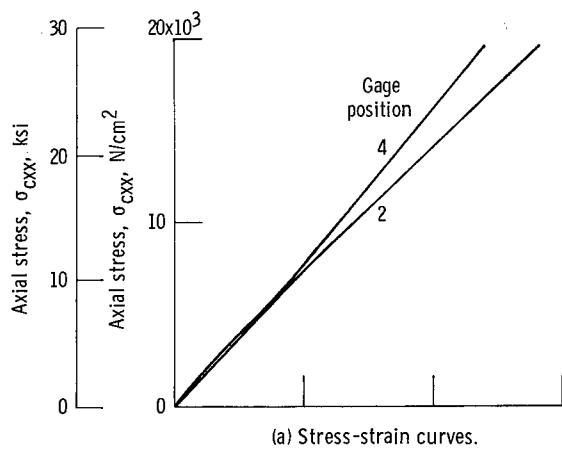
18
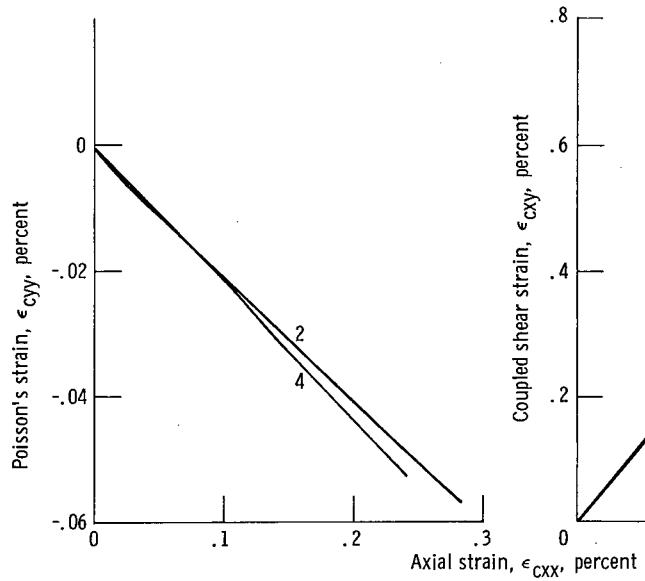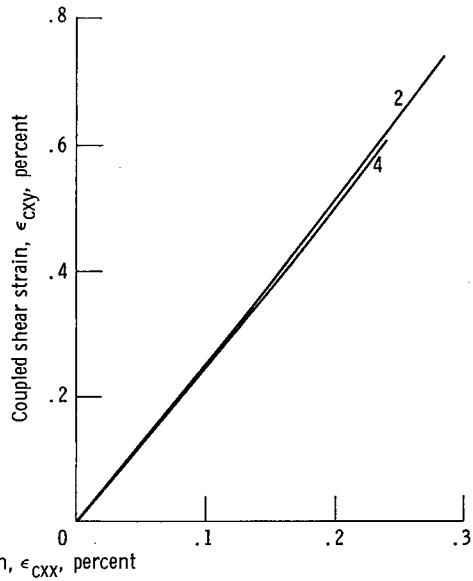
Figure 7. - Computer plotted curves through experimental data for 15° off-axis, Mod I/E fiber-composite, tensile specimen.
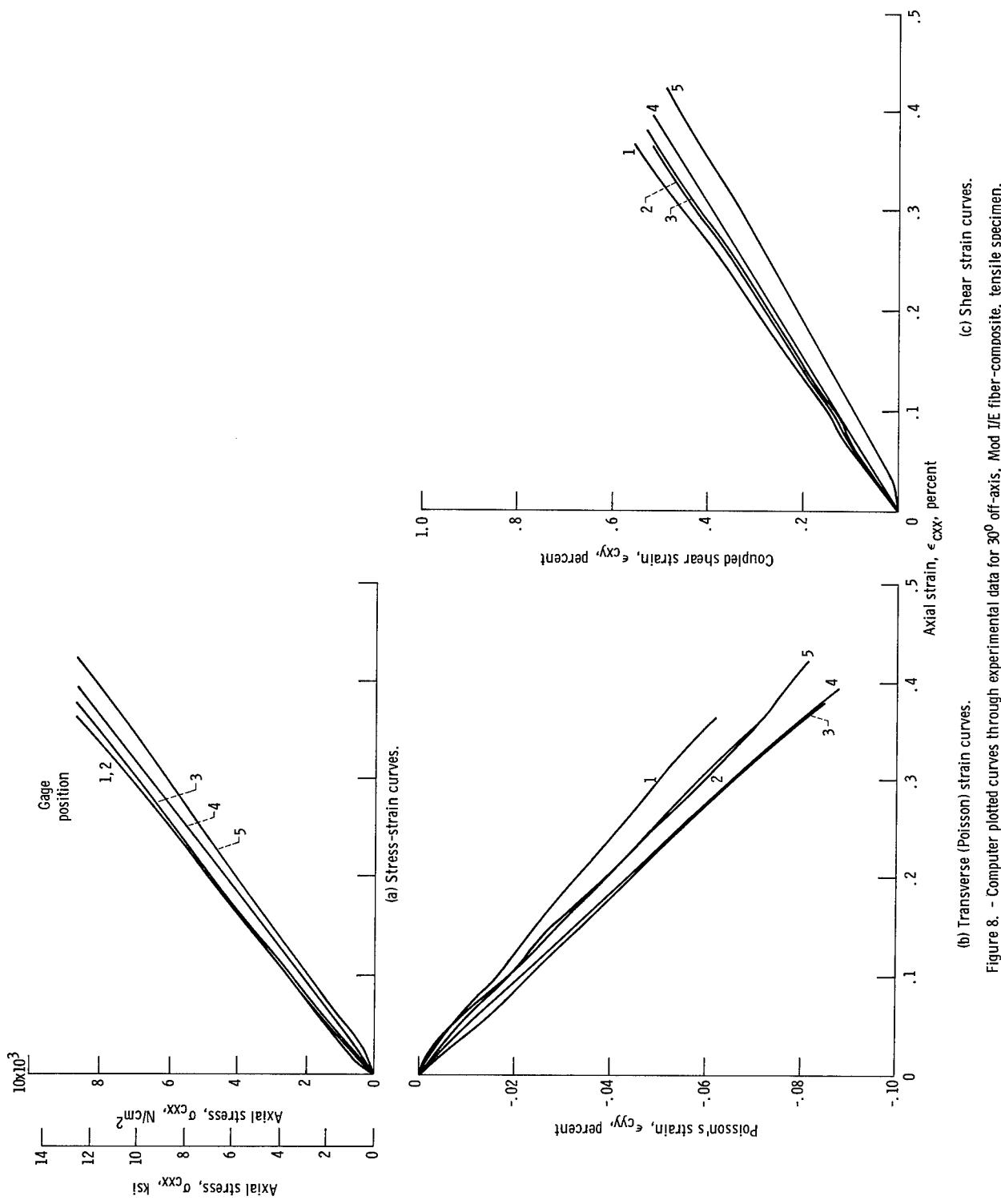
Figure 8. – Computer plotted curves through experimental data for 30° off-axis, Mod I/E fiber-composite, tensile specimen.

(a) Stress-strain curves.

(b) Transverse (Poisson) strain curves.

(c) Shear strain curves.

20
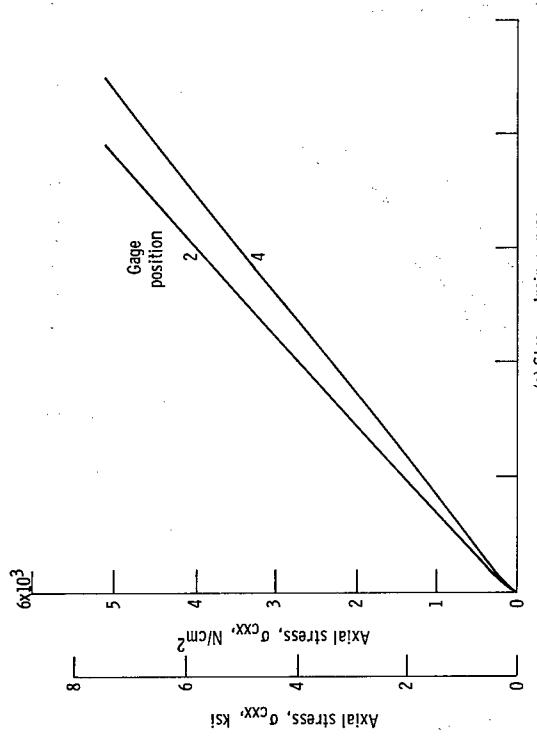
(a) Stress-strain curves.
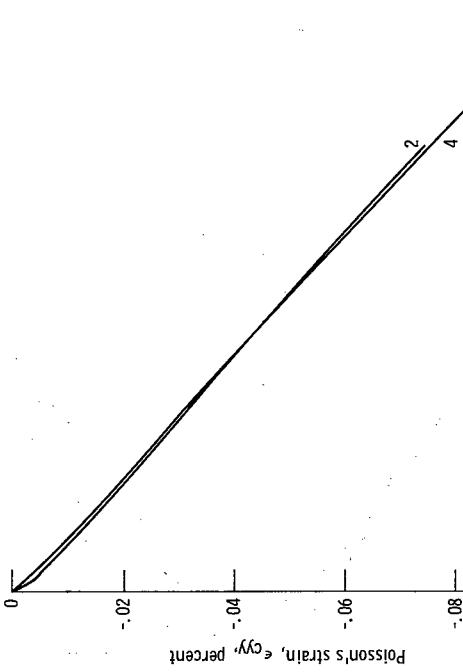
(b) Transverse (Poisson) strain curves.
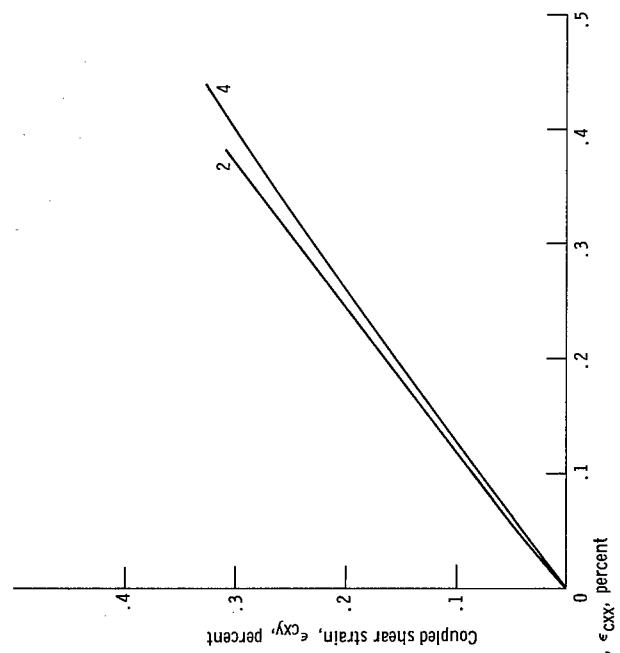
(c) Shear strain curves.

Figure 9. – Computer plotted curves through experimental data for 45° off-axis, Mod I/E fiber-composite, tensile specimen.
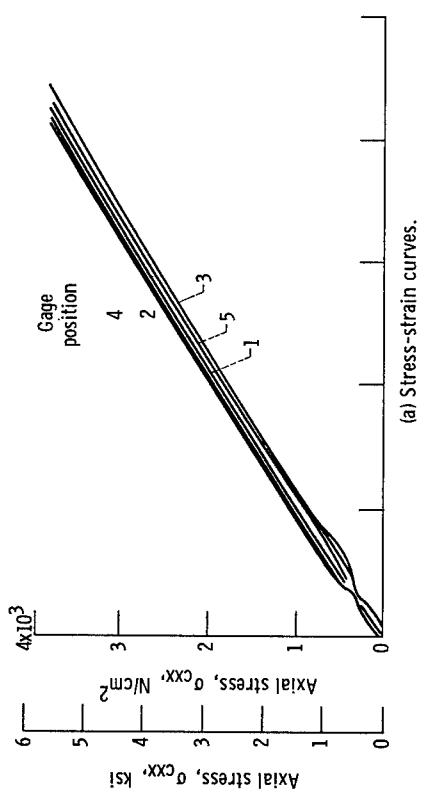
(a) Stress-strain curves.
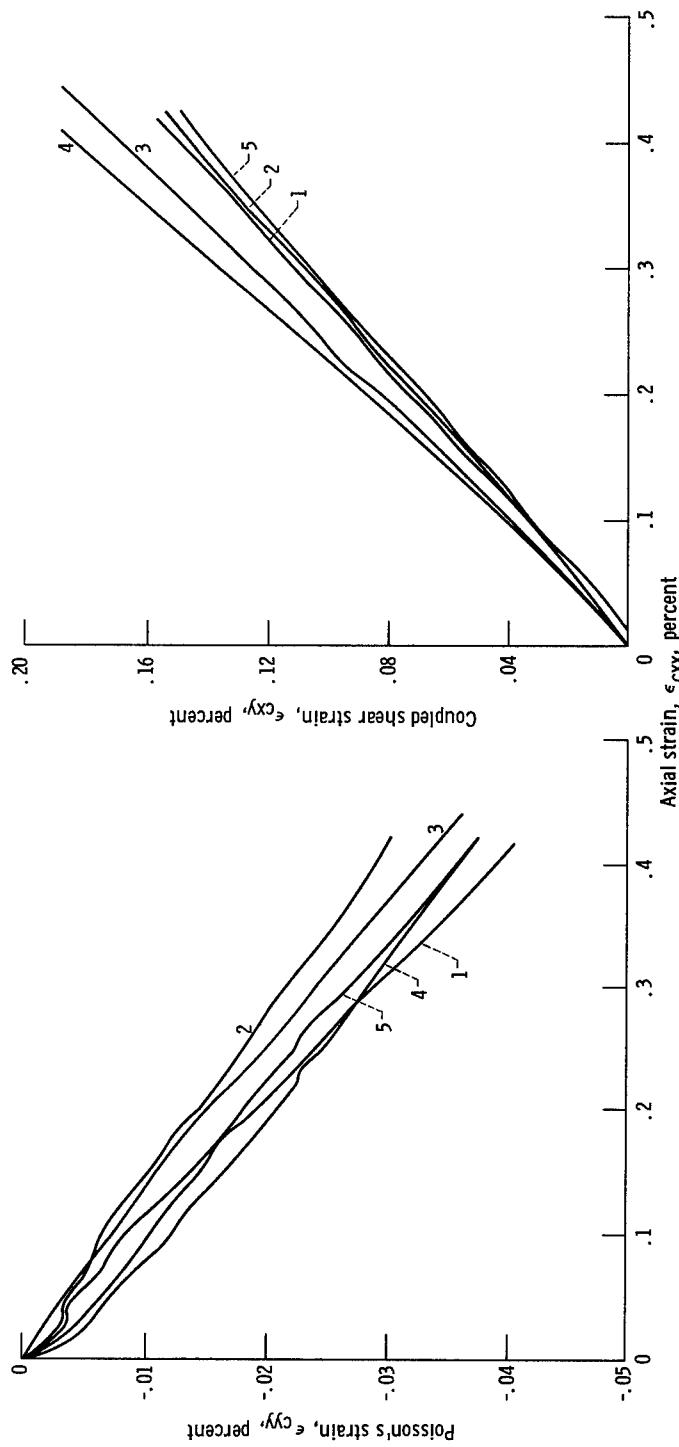
(b) Transverse (Poisson) strain curves.
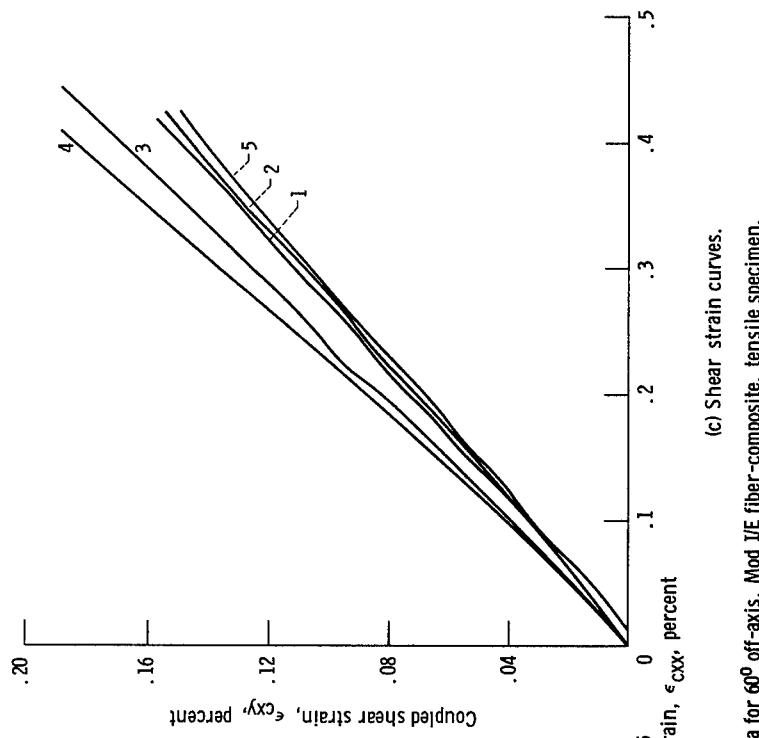
(c) Shear strain curves.

Figure 10. – Computer plotted curves through experimental data for 60° off-axis, Mod I/E fiber-composite, tensile specimen.

22

Axial stress, σ_{cxx}, N/cm^2

3.5×10^3
3.0
2.5
2.0
1.5
1.0
.5
0

Axial stress, σ_{cxx}, ksi

5
4
3
2
1
0

Gage position

2
4

(a) Stress-strain curves.

Poisson's strain, ϵ_{cyy}, percent

0
-.004
-.008
-.012
-.016
-.020

4
2

0   .1   .2   .3   .4   .5
Axial strain, ϵ_{cxx}, percent

(b) Transverse (Poisson) strain curves.

Coupled shear strain, ϵ_{cxy}, percent

.20
.16
.12
.08
.04
0

4
2

0   .1   .2   .3   .4   .5
Axial strain, ϵ_{cxx}, percent
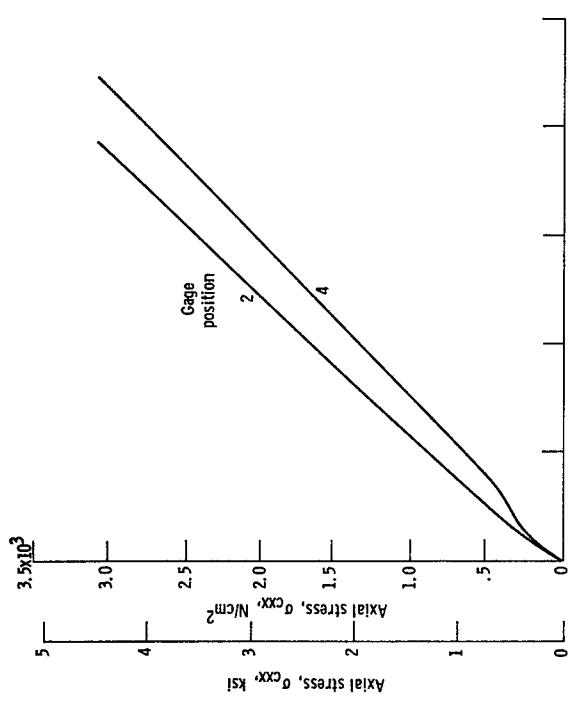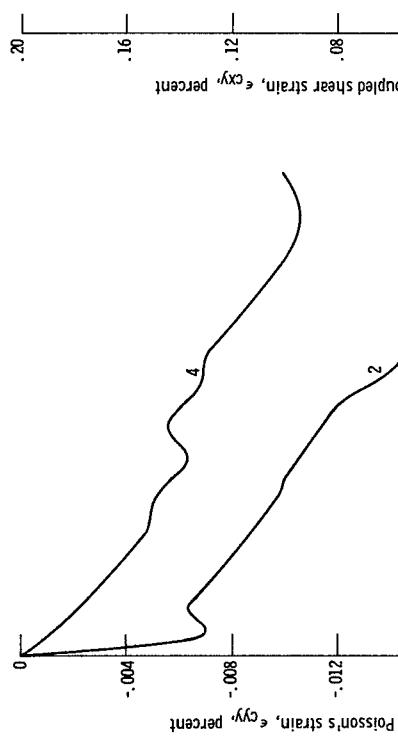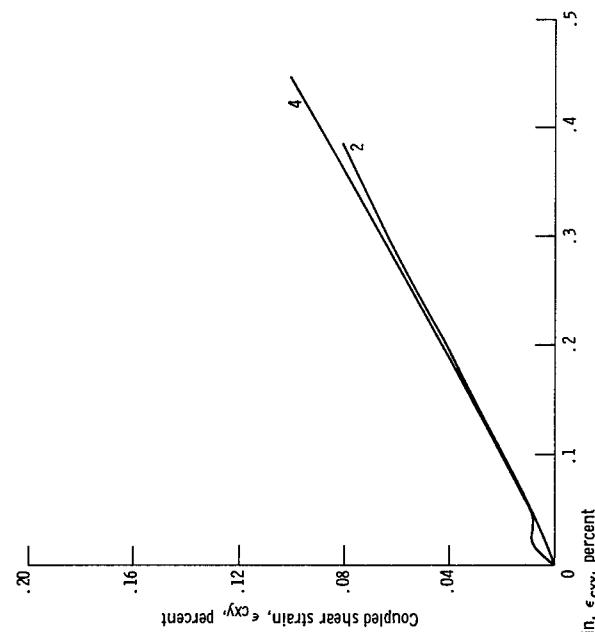
(c) Shear strain curves.

Figure 11. - Computer plotted curves through experimental data for 75° off-axis, Mod I/E fiber-composite, tensile specimen.

(a) Stress-strain curves.

(b) Transverse (Poisson) strain curves.

(c) Shear strain curves.
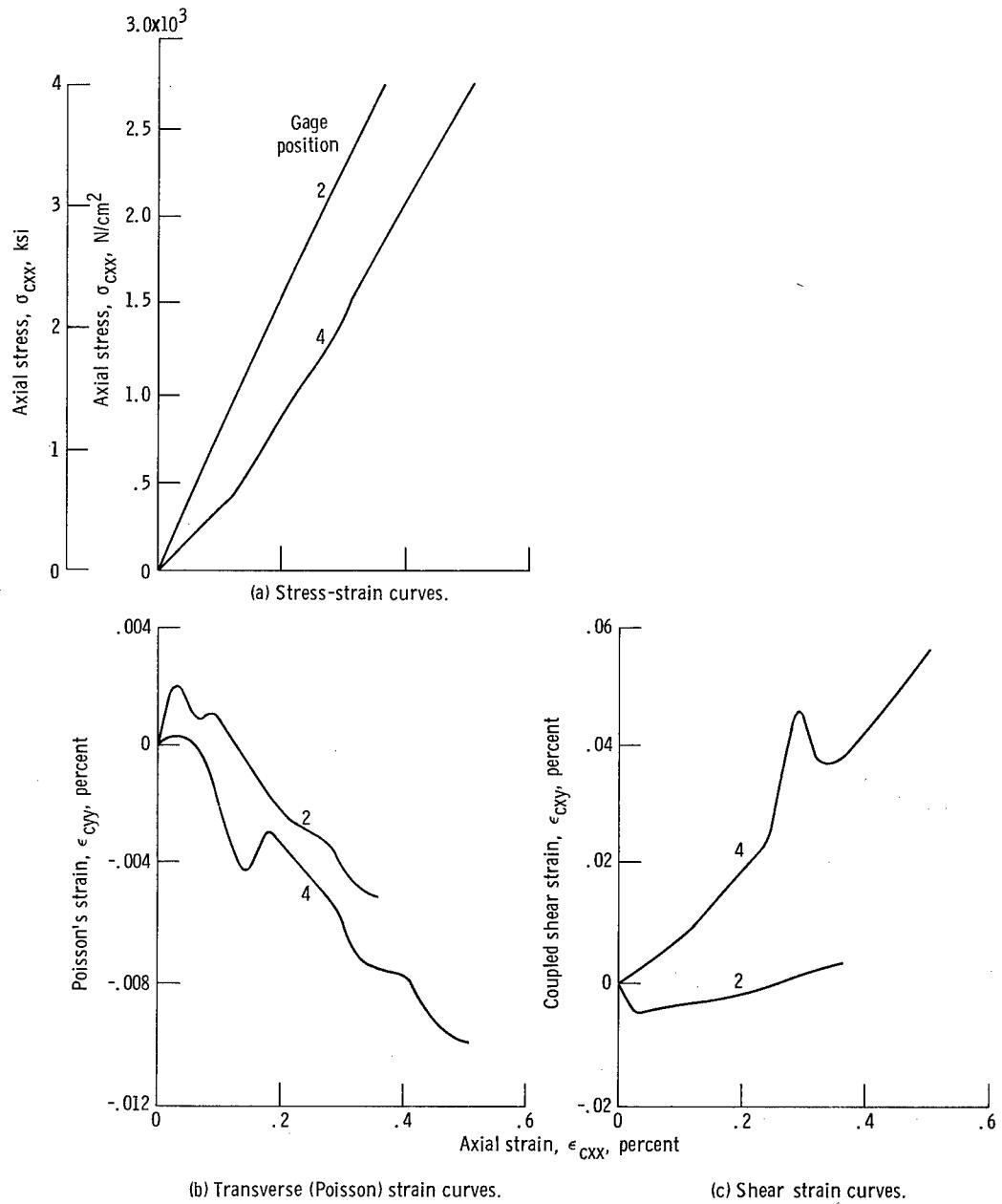
Figure 12. - Computer plotted curves through experimental data for transverse (90°) fiber-composite tensile specimen (Mod-I/E).

Figure 14. – Fractured test specimens (Mod I/E).

Figure 15. – Fractured specimen (Mod I/E) with five gages (10° off-axis).

Test angle, deg

75

60

45

30

15

10

5

0

Load angle, θ

Fiber direction

Load

Load

x

y

4 5

1 2 3

Schematic of specimen and instrumentation

At specimen midlength
Near grips (end tab)

Load angle, deg

60

30

10

30

Axial strain, ϵ_{cxx}, percent

.5

.4

.3

.2

0   12.5   50   87.5   100

Distance across specimen, percent

Measured axial strains at fracture

Gage	Load angle, θ		
	10°	30°	60°
	Fracture axial strains, percent		
1	0.320	0.365	0.417
2	.287	.365	.414
3	.336	.380	.440
4	.288	.395	.406
5	.305	.424	.421

Figure 13. – Axial strain variation at fracture across specimens of Mod I/E composite loaded at various angles from fiber direction.

25

(a) General view.

(b) Detailed view.

(c) Enlargement of detail to show fracture mode.

Figure 16. - Scanning electron photomicrographs of fractured surface of Mod I'E composite tested parallel to fiber direction.
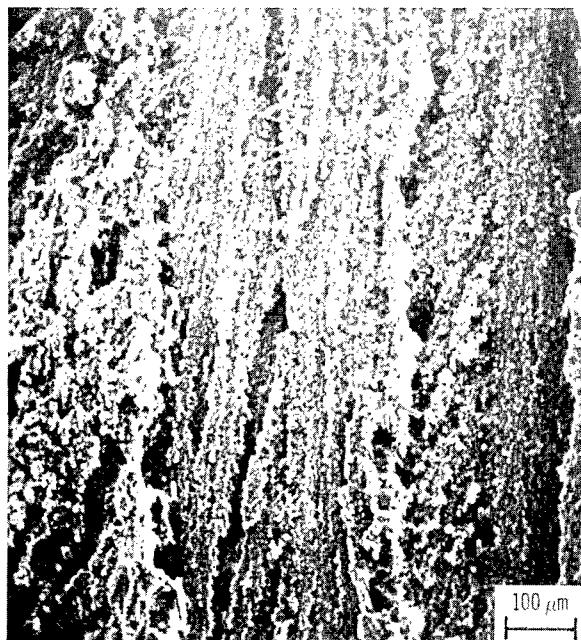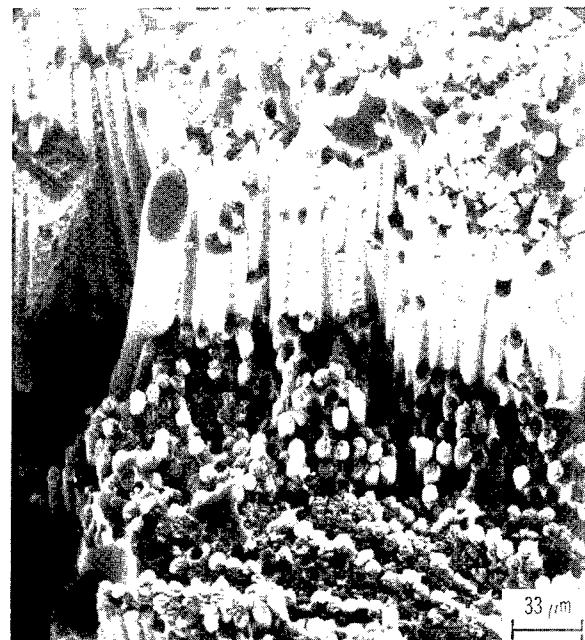
(a) General view.
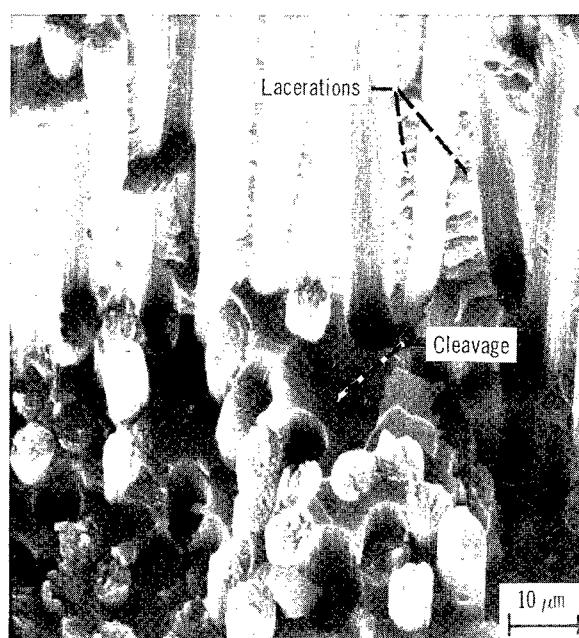
(b) Detailed view.

(c) Enlargement of detail to show fracture mode.

Figure 17. - Scanning electron photomicrographs of fractured surface of Mod I/E composite tested at 5° to fiber direction.
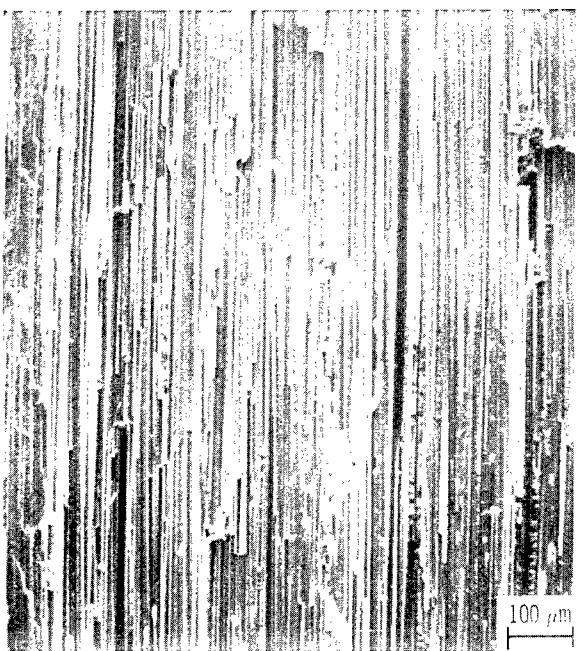
(a) General view.

(b) Detailed view.


(c) Enlargement of detail to show fracture mode.

Figure 18. - Scanning electron photomicrographs of fractured surface of Mod 1/E composite tested at 10° to fiber direction.
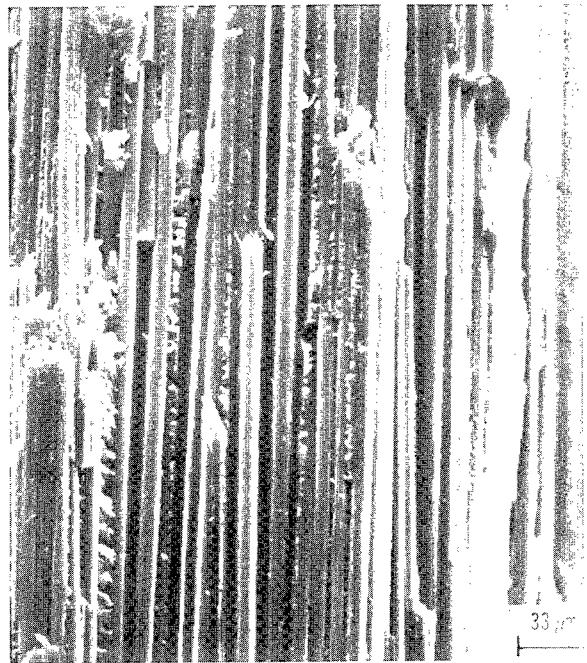
(a) General view.
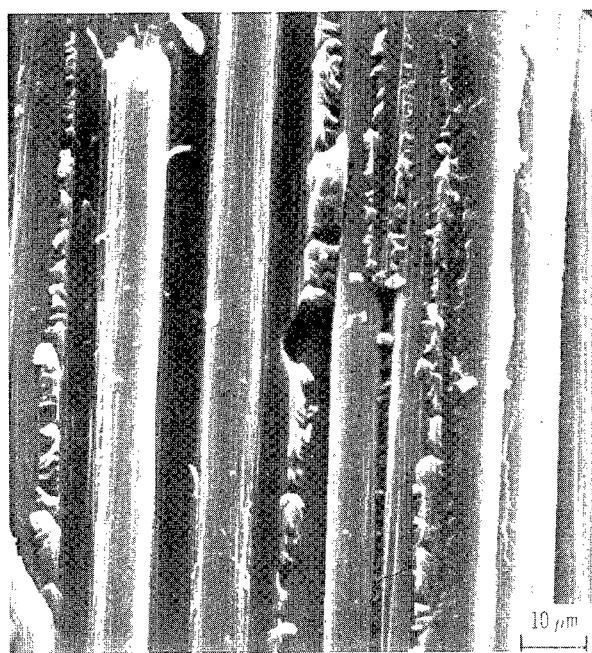
(b) Detailed view.

(c) Enlargement of detail to show fracture mode.

Figure 19. - Scanning electron photomicrographs of fractured surface of Mod I/E composite tested at 15° to fiber direction.

(a) General view.

(b) Detailed view.

(c) Enlargement of detail to show fracture mode.

Figure 20. - Scanning electron photomicrographs of fractured surface of Mod I/E composite tested at 30° to fiber direction.
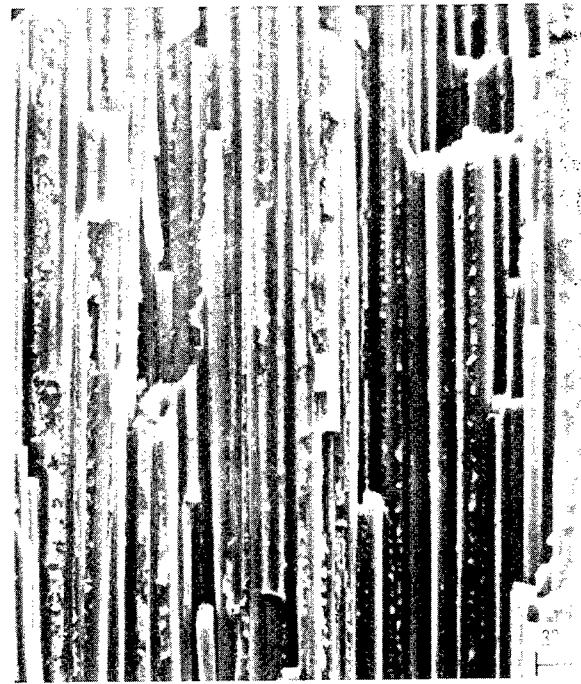
(a) General view.
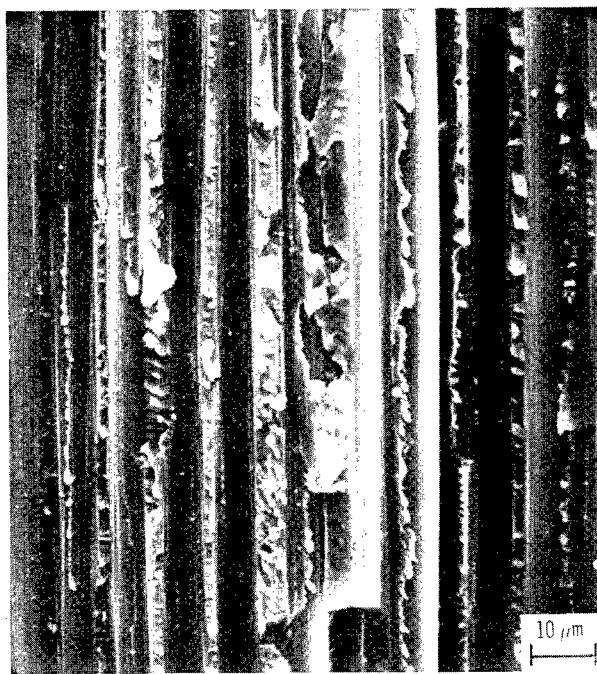
(b) Detailed view.

(c) Enlargement of detail to show fracture mode.

Figure 21. - Scanning electron photomicrographs of fractured surface of Mod I/E composite tested at 45° to fiber direction.
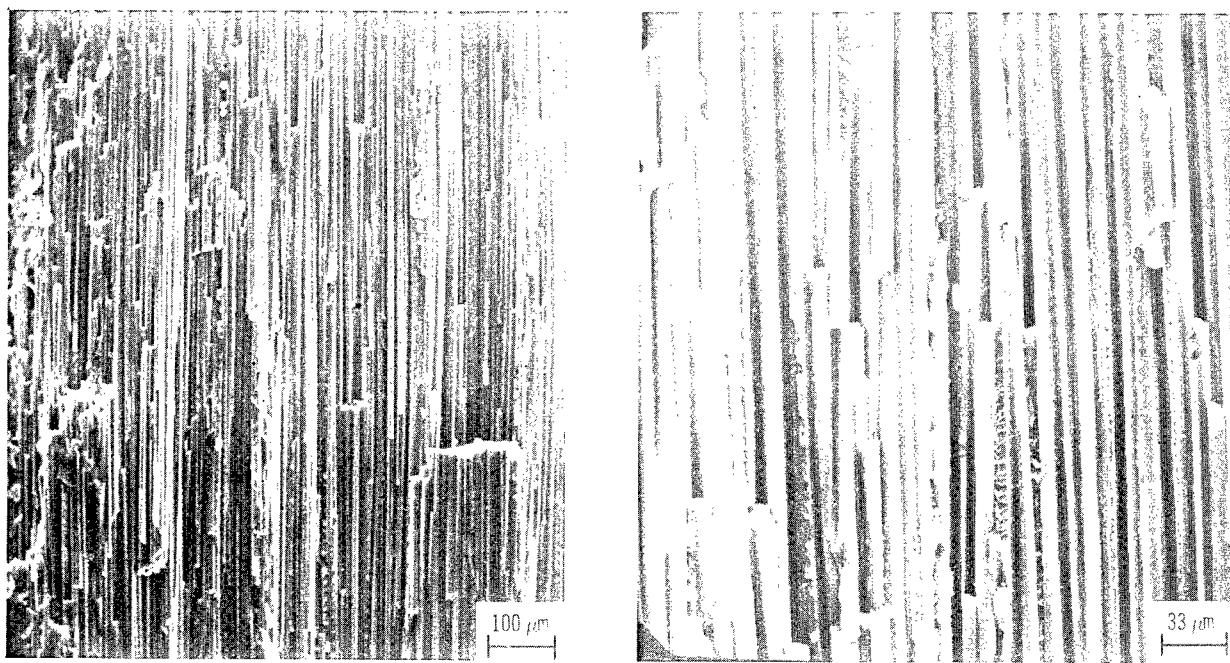
(a) General view.

(b) Detailed view.

(c) Enlargement of detail to show fracture mode.

Figure 22. - Scanning electron photomicrographs of fractured surface of Mod I/E composite tested at 60° to fiber direction.
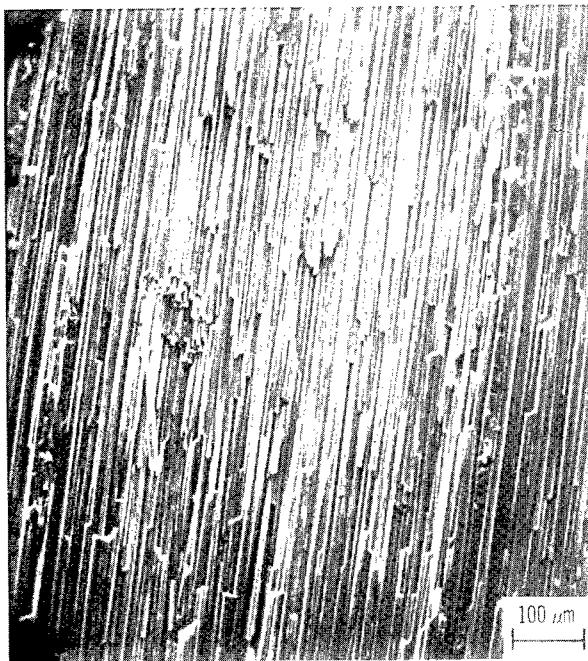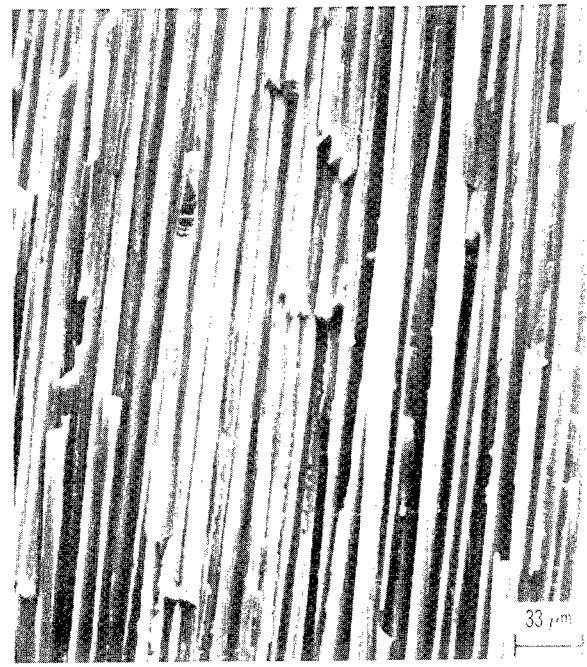
(a) General view.

(b) Detailed view.

(c) Enlargement of detail to show fracture mode.

Figure 23. - Scanning electron photomicrographs of fractured surface of Mod I/E composite tested at 75° to fiber direction.

(a) General view.

(b) Detailed view.
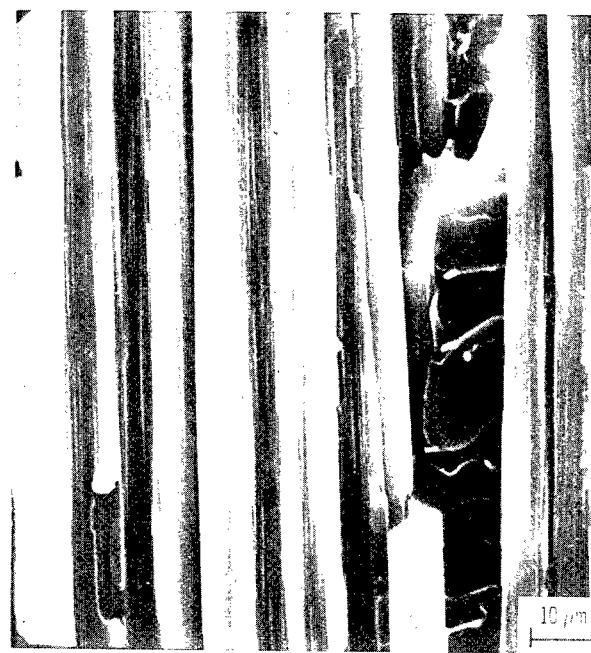
(c) Enlargement of detail to show fracture mode.

Figure 24. - Scanning electron photomicrographs of fractured surface of Mod I/E composite tested transverse to fiber direction.

1. Report No. TP-1081	2. Government Accession No.	3. Recipient's Catalog No.
4. Title and Subtitle MECHANICAL BEHAVIOR AND FRACTURE CHARACTERISTICS OF OFF-AXIS FIBER COMPOSITES I - EXPERIMENTAL INVESTIGATION		5. Report Date December 1977
		6. Performing Organization Code
7. Author(s) by John H. Sinclair and Christos C. Chamis		8. Performing Organization Report No. E-9085
		10. Work Unit No. 506-17
9. Performing Organization Name and Address National Aeronautics and Space Administration Lewis Research Center Cleveland, Ohio 44135		11. Contract or Grant No.
		13. Type of Report and Period Covered Technical Paper
12. Sponsoring Agency Name and Address National Aeronautics and Space Administration Washington, D.C. 20546		
		14. Sponsoring Agency Code

15. Supplementary Notes

16. Abstract

The mechanical behavior, fracture surfaces, and fracture modes of unidirectional high-modulus graphite-fiber/epoxy composites subjected to off-axis tensile loads were investigated experimentally. The investigation included the generation of stress-strain-to-fracture data and scanning electron microscope studies of the fractured surfaces. The results led to the identification of fracture modes and distinct fracture surface characteristics for off-axis tensile loading. The results also led to the formulation of criteria for identifying and characterizing these fracture modes and their associated fracture surfaces. The results presented and discussed herein were used in the theoretical investigation and comparisons described in Part II. These results should also provide a good foundation for identifying, characterizing, and quantifying fracture modes in both off-axis and angle-plied laminates.

17. Key Words (Suggested by Author(s)) Fiber composites; Off-axis tensile loading; High-modulus; Graphite fiber; Epoxy; Experimental; Scanning electron microscope; Stress-strain; Fracture modes; Fracture-surface characteristics	18. Distribution Statement Unclassified - unlimited STAR Category 24		
19. Security Classif. (of this report) Unclassified	20. Security Classif. (of this page) Unclassified	21. No. of Pages 35	22. Price* A03